J Nanopart Res (2023) 25:194
https://doi.org/10.1007/s11051-023-05835-x

RESEARCH PAPER

Glycol chitosan amphiphile nanotheranostic system for ultrasound-mediated localized release and biodistribution of doxorubicin

Sidra Saeed · Usama Sarwar · Masoom Yasinzai · Abida Raza

Received: 11 January 2023 / Accepted: 29 August 2023 / Published online: 14 September 2023

Abstract Ultrasound-mediated delivery has garnered attention as a noninvasive modality for localized drug delivery in cancer. Doxorubicin, a chemotherapeutic drug, shows low penetration, nonspecific distribution, and uncontrolled release. We have synthesized a hydrophobic doxorubicin (hDox)-loaded palmitoyl-modified glycol chitosan amphiphile (PmGCA) polymer-based nanotheranostic drug delivery system (hDox-NDS) for ultrasound (US)-mediated release. PmGCA encapsulates 210 µg/mL hDox in 90 ± 15 nm cationic micelles. The reappearance of the Dox fluorescence peak after 2 MHz US exposure confirms the encapsulated drug release.

hDox-NDS display a considerable drug release (~30 to 50%) over 72 h, following the Weibull model. Fluorescence microscopy shows a higher uptake of hDox-NDS (~10%) in rhabdomyosarcoma (RD) cells compared to DoxHCl. Ultrasound exposure significantly ($p < 0.001$) enhances the anticancer effect of hDox-NDS on RD cells, as shown by its lower IC_{50} value of 1.7 ± 0.05 µM compared to that of DoxHCl (2.62 ± 1.2 µM). In vivo optical imaging shows significantly lower fluorescence in the heart (~84%) and liver (~59%) compared to DoxHCl, thereby reducing side effects. This nanotheranostic hDox-NDS has been considered an effective drug delivery system, offering enhanced therapeutic effects in cancer treatment.

Keywords Glycol chitosan · Doxorubicin · Ultrasound-mediated release · Drug delivery · Optical imaging · Nanotheranostic · Cancer treatment

Supplementary Information The online version contains supplementary material available at https://doi.org/10.1007/s11051-023-05835-x.

S. Saeed
NILOP Nanomedicine Research Laboratories (NNRL), National Institute of Laser and Optronics College, Pakistan Institute of Engineering and Applied Sciences, Islamabad 46000, Pakistan
e-mail: sidra.phdns21@iiu.edu.pk

S. Saeed · M. Yasinzai
Suleiman Bin Abdullah Aba Alkhail–Centre for Interdisciplinary Research in Basic Science (SA-CIRBS), Faculty of Sciences, International Islamic University, Islamabad 44000, Pakistan
e-mail: rector@iiu.edu.pk

U. Sarwar
Department of Biotechnology, Quaid-i-Azam University, Islamabad 46000, Pakistan
e-mail: usama_sarwar@outlook.com

A. Raza (✉)
National Center of Industrial Biotechnology, University Institute of Biochemistry and Biotechnology, Pir Mehr Ali Shah Arid Agriculture University, Rawalpindi 46000, Pakistan
e-mail: abida_rao@yahoo.com

Background

In recent decades, biocompatible nanoparticle-based nanotheranostic platforms have been considered promising diagnostic and disease treatment options. Nanotheranostic has provided diagnosis, real-time drug delivery monitoring, and improved treatment efficacies in various cancers through advancements in nanomaterials and biomedical engineering techniques [1]. Ultrasound-mediated polymeric nanomicelle drug delivery has emerged as a noninvasive technique for drug delivery at the site of action [2]. Several studies have cited the use of ultrasound for doxorubicin (Dox) delivery in pancreatic, breast, and liver cancers [3]. Doxorubicin with its immense fluorescence properties [4] is an effective antitumor agent used alone or in combination to treat solid tumors (breast, bladder, ovaries, stomach, lung, and thyroid), hematological malignancies (Hodgkin's lymphoma), and soft tissue sarcomas [4, 5]. But severe side effects limit its effectiveness. When administered systemically, the drug gets dispersed in the body, leading to cardiotoxicity, hepatotoxicity, gastrointestinal toxicity, stomatitis, myelosuppression, and drug resistance [6, 7]. To overcome these side effects, a variety of Dox nanoformulation have been developed, and some are available in the market under different brand names, such as PEGylated liposomal Doxil®/Caelyx® (Janssen Products, LP., Horsham, PA, USA), Evacet® (Liposome Company Inc., Princeton, NJ), Lipodox® (Sun Pharmaceutical Industries Ltd.); non-PEGylated liposomal Myocet® (Sopherion Therapeutics, LLC, Princeton, NJ, USA); and temperature-sensitive PEGylated ThermoDox® (Celsion Corporation, Lawrenceville, NJ, US) [8]. Due to their high affinity for the lipid bilayer, liposomal formulations offer longer exposure [9], which may cause toxicity to the limbs. ThermoDox® has resolved many cytotoxicity issues, but the cardiotoxicity problem still persists.

Designing a targeted Dox delivery system is required to overcome the limitations related to Dox chemotherapy. One way to reduce the cardiotoxicity of Dox is its encapsulation in nanomicelles [10]. It has been observed that deprotonated Dox micelles or nanodroplets accumulate in the cell cytoplasm but do not reach the nuclei, which explains its low therapeutic efficacy in the absence of external stimuli [9]. Ultrasound (US) is one of the most effective noninvasive modality with high tissue penetration and has great potential for controlled drug release and improved chemotherapeutic efficacy [11]. Ultrasound can push Dox into cell nuclei due to the cavitation phenomenon [12, 13]. Ultrasound-mediated delivery works based on the temporary opening of cell membrane pores through the cavitation process, allowing drugs to enter tumor vasculature along with benefits of noninvasiveness, nontoxicity, and target specificity [14].

Glycol chitosan (GC), a derivative of chitosan, has hydrophilic ethylene glycol branches, which increase the water solubility of the polymer at neutral/acidic pH. With a deacetylation degree of 60–83%, its molecular weight ranges from 20 to 250 kDa. Modification with amine and hydroxyl groups allows the generation of a variety of derivatives of GC [15]. These GC derivatives can self-assemble with excellent drug delivery capacity. N-palmitoyl-N-monomethyl, N-N dimethyl, N-N-N, trimethyl-6-O-glycol chitosan, a self-assembling polymer, has been synthesized by attaching palmitic acid N-hydroxysuccinimide (PNS) and methylation [16]. This palmitoyl-modified glycol chitosan amphiphile (PmGCA) offers a longer plasma half-life [17]. Understudy PmGCA polymer has a quaternization level of $8.23 \pm 2.4\%$ and a palmitoylation level of $34.2 \pm 5.188\%$, hence rendering it positive and negative charges, respectively, that give unique properties to this amphiphile [18].

Ultrasound-responsive nanomicelles formulated by chitosan-based amphiphile have been vastly explored for their biosafety toward healthy tissues. Min et al. have successfully used 300-nm hydrophobic 5β-cholanic acid-modified glycol chitosan amphiphile for imaging and US-triggered docetaxel burst release using a 10-MHz frequency [19]. Additionally, Zhou et al. have developed Dox-loaded chitosan nanoparticles by incorporating a palmitic acid-Epikuron 200 system and perfluoropropane with a stabilizing aqueous solution of pluronic F68 (0.01%, w/w) and have used for controlled delivery of Dox into breast cancer cells when combined with 20-kHz ultrasound [20]. Researchers have reported good drug loading ability and enhanced US imaging by stimulating the drug release from nanobubbles. These studies show that US-responsive glycol chitosan-based nanoformulation may have a wide range of potential applications in medicine and must be studied in different systems while using a variety of polymers [21]. However, no data on PmGCA in combination with US has been reported.

We hereby proposed the encapsulation of hydrophobic doxorubicin in N-palmitoyl-N-monomethyl,

N-N dimethyl, N-N-N, trimethyl-6-O-glycol chitosan (PmGCA) to prepare a nanotheranostic drug delivery system (NDS) that can be externally stimulated through ultrasound for enhanced penetration and drug release at the site of action. Moreover, it can be tracked through optical imaging for drug distribution, and it is also expected that hDox-NDS nanotheranostic micelles may offer lower toxicity toward the heart and other organs. In this study, we have reported for the first time that PmGCA has been used in combination with the low frequency of ultrasound and low dose of the fluorescent drug doxorubicin.

Materials

Doxorubicin HCl (44583), Hanks buffer salt solution, (HBSS) (11140007), phosphate buffer saline, (PBS) (4417), acetone (65050), triethylamine, (TEA) (121-44-8), trypsin-EDTA 10x (T4174), and trypan blue 0.4% (15250-061) were purchased from Sigma Aldrich (St Louis, MO, USA). Dulbecco's Modified Eagle Medium, (DMEM) (1732501), penicillin and streptomycin (15140-122), heat-inactivated fetal bovine serum, (FBS) (10270-106), and phytohemagglutinin, (PHA) (00-4977-93) were purchased from Gibco-Life Technologies, NY, USA. Ultrapure agarose, Invitrogen (16500), and Sephadex G-25 were purchased from GE Healthcare Bio-Sciences AB (Uppsala, Sweden). For cytocompatibility study, human rhabdomyosarcoma (RD) cells ATCC CCL 136 were provided by the National Institute of Health (NIH) (Islamabad, Pakistan). Other reagents related to cell culture were purchased from Gibco-Life Technologies (Thermo Fisher Scientific, NY, USA) or Sigma-Aldrich (USA).

Methods

Preparation of hDox-loaded nanotheranostic micelles

Palmitoyl glycol chitosan amphiphile (PmGCA) polymer with a quaternization level of 8.23 ± 2.4% and a palmitoylation level of 34.2 ± 5.2% was synthesized by following the method as stated in our previous work [22]. Briefly, sodium bicarbonate (376 mg) and hydrolyzed GC (500 mg) were mixed in a flask containing water: ethanol solution. Subsequently, gas chromatography of the sodium bicarbonate solution and palmitic acid N-hydroxysuccinimide solution was conducted for 72 h. The resulting product was separated by ethanol evaporation and re-dispersed in distilled water. The excess palmitic acid N-hydroxysuccinimide was removed by extracting it three times with diethyl ether, and the mixture was dialyzed for 24 h against distilled water. The dialysate was then dried through freeze-drying. The mixture was dialyzed against 5 L of distilled water for 24 h, quaternization was carried out by dispersing palmitoyl GC in 25 mL of N-methyl-2 pyrrolidone, ethanolic solution (5 mL) was prepared by dissolving sodium hydroxide (40 mg) and sodium iodide (45 mg) to palmitoyl GC, and then methyl iodide (1 g) was added and kept under nitrogen gas for 3 h in dark. Diethyl ether was used to precipitate quaternary ammonium product, and dialysate was purified through Amberlite-96 resins. Final dialysis results into cotton-like solid palmitoyl glycol chitosan amphiphile (PmGCA) were obtained after freeze-drying with a molecular weight of 178,000 $gmole^{-1}$.

In this study, DoxHCl was converted into hydrophobic Dox (hDox) following the previously reported method [23]. Briefly, DoxHCl (3 mg) was dissolved in a 1:1 ratio of methanol: chloroform (1 mL, v/v), followed by the addition of triethylamine in a molar ratio of 1:3 and incubated overnight at room temperature till solvent evaporation. This hDox (300 µg) was added to a 2 mg/mL aqueous solution of PmGCA. The mixture was sonicated for 20 min at 70% amplitude with a 6-mm diameter probe (SONIC Vibra Cell, USA). The formulation was passed through a G-25 Sephadex column to remove unencapsulated hDox from hDox-NDS delivery system.

hDox-NDS formulation optimization

The nanoformulation was optimized by Design expert® (software 7.0 Stat-Ease, Inc., Minneapolis, MN) using the central composite design (CCD) for the ratio of ingredients as independent factors against dependent responses [24, 25]. Response surface methodology (RSM) was used to evaluate the effects of factors on responses such as concentration of hDox, glycol chitosan amphiphile, probe amplitude, and sonication time against dependent responses of particle size,

polydispersity index (PDI), zeta potential, and encapsulation efficiency. The most appropriate formulation was selected based on size, with the minimum PDI and highest encapsulation efficiency.

Size distribution, morphology, and serum stability of hDox-NDS

The hydrodynamic size, mean diameter, zeta potential of hDox-NDS nanomicelles, and population distribution (as polydispersity index) were measured using dynamic light scattering (DLS). Measurements were recorded at 25 °C using Microtrac Nanotrac Wave II (USA) in triplicate. hDox-NDS nanomicelle wet stability was observed for 3 months at 4 °C. Confirmation of encapsulation was done through Raman spectroscopy at room temperature with the following parameter settings: 785 wavelength scan, 20 °C, 5–300-mV power supply, and 5–30-s integration time (Raman System Peak Seeker; PRO-785; Microscope RSM-785, AGILTRON, USA). For serum stability, hDox-NDS was incubated with human serum in a 1:1 at 37 °C, and size was measured at the 0.5, 1, 2, 3, 4, 6, and 8 h time points. DLS was done after US application to monitor the effects of US on particle size and PDI of the formulation. The fluorescence properties of Dox can be utilized for encapsulation confirmation. Once the drug is encapsulated, its fluorescence might get trapped inside micelles; hence, no signatory peaks through photoluminescence (PL) can be seen. This quenching phenomenon has been studied for hDox-NDS nanomicelles before and after US exposure as a confirmation of encapsulation and subsequent drug release. Excitation and emission spectra were recorded at 485 and 550 nm, respectively, with a helium-cadmium laser of 40 MW power with Dongwoo Optron (Model no.DM. 3201, Korea). The encapsulation efficiency (%) was calculated with hDox calibration curve at 0–100 µg/mL concentrations at a wavelength of 485 nm using spectrophotometer (U-2900 UV-VIS Spectrophotometer-HITACHI High-Tech Science, λ = 200–1100 nm) using the formula:

$$\text{Encapsulation efficiency (\%)} = \left(\text{Qtotal} - \frac{Q\text{free}}{Q\text{total}} \times 100\right)$$

Hemocompatibility of hDox-NDS micelles

The hemolytic activity of hDox-NDS, PmGCA, and DoxHCl was evaluated with some modifications in the protocol [26, 27]. RBCs were washed with HBSS 3 times. The erythrocytes concentration was adjusted to 10% by volume with HBSS and incubated with hDox-NDS formulation in different concentrations ranging from 1 to 10 µM for 1 h at 37 °C. Cell suspensions were centrifuged at 100 g for 5 min. Hemolytic activity was assessed from hemoglobin release at 576 nm using microplate reader (BioTek, USA).

$$\text{Hemolysis (\%)} = \left(\frac{\text{Absorbance of sample} - \text{Absorbance of negative sample}}{\text{Absorbance of positive sample} - \text{Absorbance of negative sample}} \times 100\right)$$

Ultrasound parameter optimization and phantom model

Ultrasound conditions were optimized using an 18 × 23.7-mm 1.5–4-MHz frequency transducer (3Sc-RS probe) at a 90° field of view with a field depth of 30 cm. The transducer was driven with an electric signal generated by the LOGIQ e Ultrasound System (S.No.220v17370469 GE, USA). To avoid sound wave reflection, a heat absorbing pad was kept below the cell culture plate. The effect of ultrasound was measured with a constant exposure time of 30 s for in vitro assays and 1 min (60 s) for in vivo assays. A mechanical index (MI) value of 1.2 was kept constant with a specific ultrasound frequency of 2 MHz for each experimental setup.

A gel-based phantom was designed to examine the potential of US-mediated extravasation of hDox-NDS following the protocol with some modifications [28, 29]. Briefly, the phantom was made from 2.5% (w/v) low melting point pure agarose gel of 1-mm pore size and a depth of 1.5 cm. A solution of hDox-NDS (210 µg/mL) was injected into phantom channels. Using an 18 × 23.7-mm transducer (3Sc-RS probe) from the GE Healthcare LOGIQTM e ultrasound system, a 2 MHz frequency was applied at a 90° field of view and a depth of 30 cm. Images were taken in conventional B mode.

US-mediated in vitro release of drug from hDox-NDS micelles

The dialysis membrane technique was used to determine the hDox release from hDox-NDS with and without ultrasound exposure. The nanoformulation (1 mL) was dialyzed against 100 mL of PBS (pH 7.4) by a dialysis membrane (MW cutoff of 12 kDa, Sigma-Aldrich). The hDox release from nanomicelles was measured at 37 °C with continuous stirring at 50 rpm at predetermined time points of 0.5, 1, 2, 3, 4, 5, 6, 24, 48, and 72 h. Absorbance was measured at 485 nm using a microplate reader (Epoch2 BioTek, USA). At four time points (1, 3, 6, and 24 h), US was applied with the 1.5–4-MHz transducer (3Sc-RS probe) probe by setting it to 2 MHz for 60 s at a 90° field of view with a field depth of 30 cm. The transducer was driven with an electric signal generated by the LOGIQ e Ultrasound System (S.No.220v17370469 GE, USA). The percent cumulative release for both the US- and no-US–mediated profile was recorded. The percentage difference in cumulative release caused by the US was calculated at 1-, 3-, 6-, and 24-h time points [30]:

$$\text{Cumulative release (\%)} = \left(\frac{\text{US mediated PCR of hDox} - \text{NDS(t)} - \text{No US PCR of hDox} - \text{NDS(t)}}{\text{No US PCR of hDox} - \text{NDS(t)}} \right) \times 100$$

where cumulative release caused by US:

$$\Delta \text{ Release (time)} = \left\{ \frac{(\text{US mediated PCR(t)} - \text{NoUS PCR (t))}}{\left(\text{No US PCR(t)}\right.} \times 100 \right\}$$

where PCR and *t* stand for percent cumulative release and time point, respectively. To study hDox release mechanism from hDox-NDS, six different kinetic models (zero order, first order, Higuchi, Hixson-Crowell, Weibull, and Korsmeyer-Peppas) were applied to fit the experimental data.

Effect of US on hDox-NDS uptake in RD cells

Human rhabdomyosarcoma (RD) cells were grown with 10% heat-inactivated FBS, penicillin (100 U/mL), and streptomycin (100 mg/mL) in DMEM and kept in a CO_2 incubator (Thermo Fisher Scientific, OH, USA), until 90% confluency [16]. Cells were seeded in six-well plates at a density of 1×10^6 per well. Cells were kept at 37 °C, 5 % CO_2 for 24 h before exposure to hDox-NDS. DoxHCl and hDox-NDS (5 μM) were added to each well and incubated at 37 °C for 30 min. Each well was exposed to constant US exposure of 30 s with a mechanical index value of 1.2 [31], at 2-MHz frequency, with a depth of 51 db (fresh media was added before US application to prevent cavitation attenuation due to high concentration of CO_2 accumulation). To avoid sound wave reflection, a heat absorbing pad was kept below the cell culture plate. After 4 h of incubation, cells were washed with PBS to remove residual drug. For fluorescence measurement, cells were examined using fluorescence microscopy (EVOS Cell Imaging Systems, Life Technologies-Thermo Fisher Scientific, USA). Fluorescence intensities were further analyzed for corrected total cell fluorescence (CTCF) using Image J software [32] (win-64 FIJI) through a formula:

$$\text{CTCF} = \text{Integrated Density} - (\text{Area of selected cell} \times \text{Mean background fluorescence})$$

Effect of ultrasound on hDox-NDS micelles macrophage uptake

Macrophages were isolated according to the protocol described by Lefort, Craig T., and Minsoo Kim [33] with modifications. Briefly, the fresh blood was collected in heparin and diluted with sterile 10 mL PBS followed by the addition of histopaque and centrifugation at 1500 rpm, 20 °C for 20 min. Isolated mononuclear cells were washed twice with PBS. The cells were incubated overnight at 37 °C in CO_2 (5 %) with fresh cell culture media and phytohemagglutinin (PHA). Cells were seeded in six-well plates at a seeding density of 1×10^6 cells/mL. DoxHCl and hDox-NDS nanomicelles (5 μM) were added to the macrophage monolayers and incubated for 30 min before US application. After 4 h of incubation, the cells were washed with PBS to remove any unabsorbed drug and examined under fluorescence microscopy (EVOS Cell Imaging Systems, Life Technologies-Thermo Fisher Scientific, USA).

Ultrasound-mediated anticancer effect of hDox-NDS

RD cells seeded at a density of 1×10^6 cells/well in a flat bottom 96-well plate were incubated for 24 h in CO_2 incubator (5%). Cells were washed with PBS and treated varied concentrations (0.05–5 µM) of with hDox-NDS and DoxHCl to evaluate cytotoxicity (untreated cells were used as a negative control). Cells were exposed to 2-MHz (1.2 MI) ultrasound for 30 s and incubated for 48 h. MTT (3-(4, 5-dimethylthiazol-2-yl)-2,5-diphenyl-2H-tetrazolium bromide) (5 mg/mL) was added to each well and incubated for 4 h. The resulting formazan crystals were dissolved in 200 µL of DMSO and incubated for 30 min at room temperature. The absorbance of each well was measured at a wavelength of 570 nm using an ELISA plate reader (Model FDx800, Biotek, VA, USA). Half-maximal inhibitory concentration (IC_{50}) was calculated using GraphPad Prism.

For cell survival study, the cells were seeded in six-well plates for survival study and incubated with hDox-NDS/DoxHCl for 6 h. Cells were then exposed to US for 30 s. The trypan blue dye exclusion test was used to determine the survival of the cells. By combining 100 µL of cell suspension with an equivalent amount of 0.3% trypan blue solution in PBS, the trypan blue dye exclusion test was carried out. To determine the approximate number of intact viable cells after a 4-min incubation period at room temperature, the cells without the dye (trypan blue) were counted using a hematocytometer under a microscope [34].

In vivo biodistribution of hDox-NDS nanomicelles

BALB/c mice ranging in weight from 18 to 30 g were purchased from the National Institute of Health (NIH) in Islamabad, Pakistan. Ethical approval was taken from the NILOP ethical approval committee under code No (No Sec-44 (1/16/A547)) for working with animals.

Animals were divided into three groups and injected with 0.05 µg/g of DoxHCl/hDox-NDS nanomicelles through the tail vein for biodistribution study. One group was used as a control. One of the two groups was sonicated, while another was not (Table S2). Animals were sacrificed a half-hour after the sonication process was finished, the organs were removed, and the fluorescence signals from the organs were examined using the in vivo imaging system at excitation filter 535/45, and emission filter 605/50 with the Bioautomatic MultiSpectral Light Source (UVP iBox® Explorer^2 Imaging Microscope, Analytik Jena, CA (USA). Following imaging, organs were cleaned with PBS to prevent any erroneous blood fluorescence and fixed in a 10% formaldehyde solution for histological study. Fluorescence intensities were further analyzed using Image J software [32] version Win-64 FIJI using the formula for corrected total fluorescence.

Histopathology examination

The mice organs (brain, heart, liver, kidney, lungs, and spleen) were collected for histopathology examination. All tissues were fixed with paraformaldehyde (4%) and embedded in paraffin. The embedded organs were sliced into 5-µm thickness, fixed on a glass microscope slide, and stained with hematoxylin and eosin (H&E) for microscopic observations.

Statistical analysis

Statistical analysis was performed using GraphPad Prism 8 and Origin Pro 8 software. All experiments were performed in triplicates.

Results and discussion

The detailed scheme of hDox-NDS nanomicelles is presented in Fig. 1.

Optimization and preparation of hDox-NDS nanomicelles

Formulation has been theoretically optimized using simulation software based on RSM plots for the most suitable concentrations of ingredients (Fig. 2A). Doxorubicin and polymer ratios, amplitude, and sonication time are the variable factors that can affect particle size, zeta potential, and polydispersity index and encapsulation efficiency. Reducing the concentration of hDox and increasing polymer ultimately result in larger particle size and vice versa. An optimal area is selected where small particle sizes offer maximum capacity for encapsulation and less population heterogeneity. Predicted values have helped us in

reproducing a hassle-free formulation in a wet lab with more stability, the required size, and zeta potential. The experimental values (size, zeta potential, and PDI) of synthesized formulation were very close to the predicted values of size 91 ± 15 nm, zeta potential of +32 ± 5 mV, and PDI of less than 1 which offers 70% encapsulation efficiency (Table 1). Esmaeilzadeh-Gharedaghi et al. (2012) have confirmed that parameters (concentration, sonication time, and amplitude) have a direct effect on nanoparticle size, PDI, and encapsulation of the drug. Optimal conditions for minimum size can be obtained with high amplitude and sonication time [35].

Characterization of hDox-NDS cationic micelles

Dynamic light scattering confirms the hydrodynamic size distribution of 90 ± 15-nm hDox-NDS nanomicelles with a polydispersity index of 0.224 ± 0.01 and a zeta potential value of +30 ± 5 mV. A low PDI value shows a homogenous population of the particles (Fig. 2B). PmGCA has shown the unique property of self-assembling into micelles at room temperature, encapsulating hydrophilic and hydrophobic drugs and actively delivering these drugs through biological barriers, enhancing their bioavailability. Because of its amphiphilic nature, PmGCA can result in both anionic and cationic-charged formulation. DLS shows a slight increase in size and PDI after US (Fig. 2C). This increase indicates a US trigger release of payload on application resulting in increased PDI and size. In this study, PmGCA produced a cationic formulation (+ ζ) of hDox in contrast to our previously published study [22] which reported an anionic formulation −25 ζ) when DoxHCl was encapsulated [22]. hDox-NDS cationic surface potential and electrostatic stability give it an advantage in interacting with negatively charged cell surfaces. The drug's hydrophobicity or hydrophilicity has a significant impact on size as reported earlier by Uchegbu et al. (2021). They have also reported 100–500-nm micelles for encapsulation of hydrophobic cyclosporine A in GCPQ polymer after 20 min of probe sonication for ocular inflammation formulation [36].

Raman vibrational modes reveal DoxHCl peaks at 162.2 cm^{-1}, 206.1 cm^{-1}, 342.7 cm^{-1}, 463.5 cm^{-1}, 499 cm^{-1}, 522.8 cm^{-1}, 599 cm^{-1}, 793.2 cm^{-1}, 868 cm^{-1}, 910 cm^{-1}, 985 cm^{-1}, 1085 cm^{-1}, 1202.8 cm^{-1}, 1288.5 cm^{-1}, 1424.8 cm^{-1}, 1461 cm^{-1}, 1578 cm^{-1}, and 1646 cm^{-1}, whereas these peaks disappear in case of hDox-NDS. hDox-NDS on other hand peaks at 151.9 cm^{-1}, 300.3 cm^{-1}, 762.6 cm^{-1}, 796.4 cm^{-1}, 838.5 cm^{-1}, 1016.4 cm^{-1}, and 1269.6 cm^{-1} are being

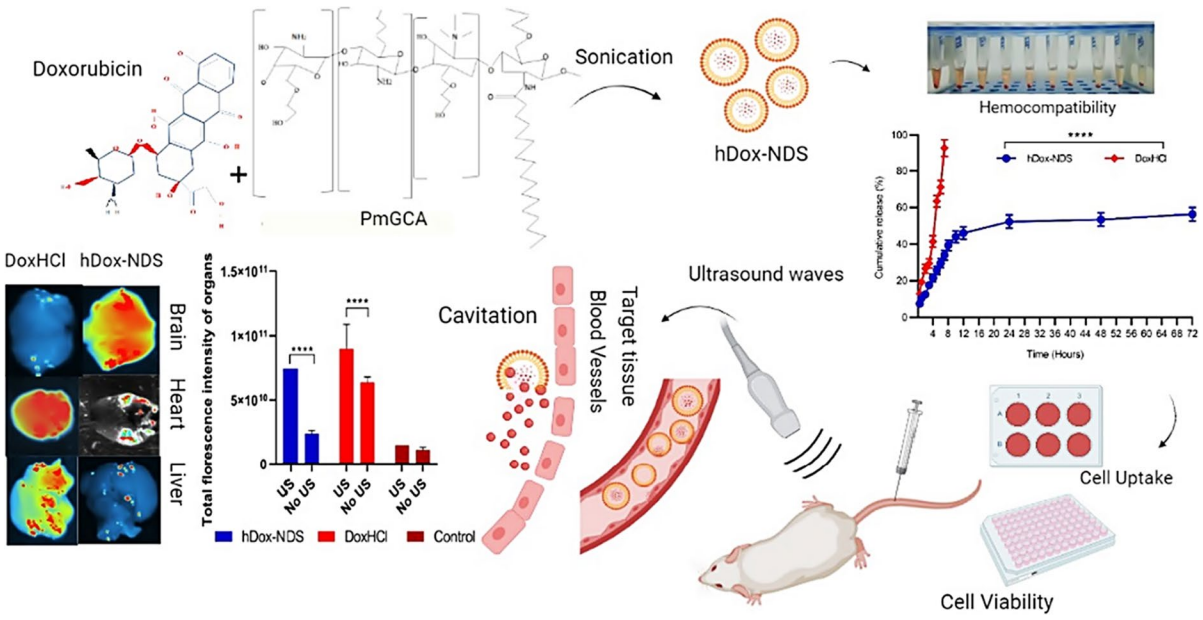

Fig. 1 Graphical abstract of ultrasound-mediated localized release and biodistribution of doxorubicin from glycol chitosan amphiphile nanotheranostic system

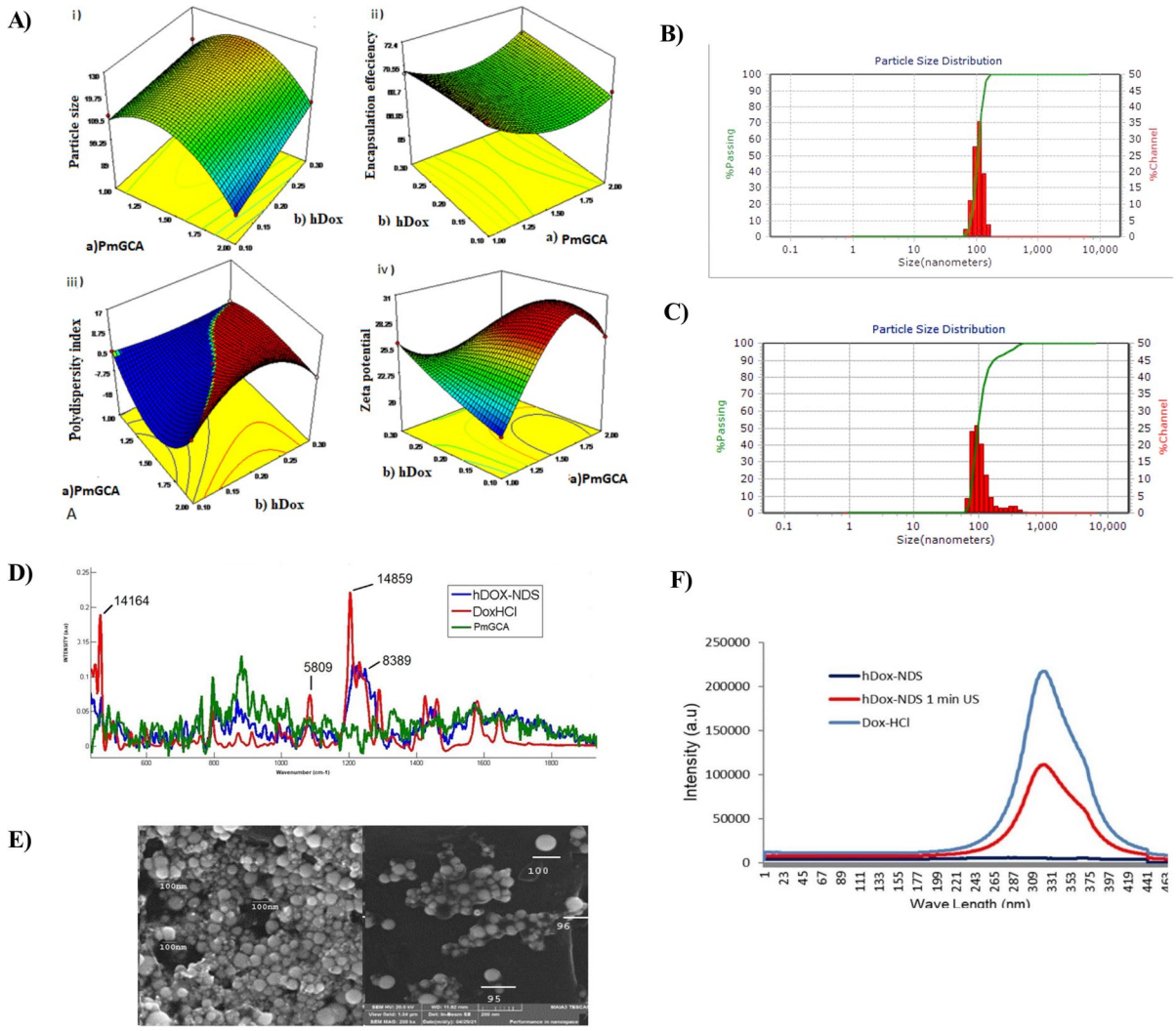

Fig. 2 Optimization and characterization of Dox delivery system. **A** RSM plots of the hDox-NDS showing the effect of independent factors on (i) size, (ii) encapsulation efficiency, (iii) polydispersity index (PDI), and (iv) zeta potential. **B** Dynamic light scattering size 90 ± 15 nm. **C** DLS after US exposure showing 116 nm size. D Raman spectroscopy showing disappearance of distinct peaks of DoxHCl in hDox-NDS confirming successful encapsulation. **E** Scanning electron microscopy images of hDox-NDS. **F** Photoluminescence spectra of hDox-NDS, DoxHCl, before and after US

observed. The disappearance of distinct peaks of the hDox in hDox-NDS Raman spectra confirms the successful encapsulation of doxorubicin and formation of nanomicelles (Fig. 2D). SEM also confirms that the size is less than 100 nm (Fig. 2E). X-ray diffraction (XRD) and Fourier transform infrared spectroscopy (FTIR) analysis of DoxHCl and hDox-NDS nanomicelles are shown in Fig. S1A-B and Table S1 indicating the positioning of bonds in FTIR analysis of formulation.

Fluorescence quenching as a confirmation of Dox encapsulation

The fluorescence property of Dox can be utilized for confirmation of its encapsulation in a drug cargo. The disappearance of the peak ($\lambda_{em,}$ 485) in photoluminescence spectra indicates fluorescence quenching of Dox which is directly related to successful encapsulation of drug into PmGCA nanomicelles (Fig. 2F). Though hDox encapsulation efficiency can

Table 1 Optimization parameters (size, zeta potential, PDI) of hDox-NDS nanomicelles

No. of formulation (drug: polymer)	Size distribution (nm)	Zeta potential (mV)	Polydispersity index
300 µg:2 mg	90 ± 1.528	30 ± 2.082	0.226 ± 0.003
300 µg:1 mg	90.3 ± 2.066	33 ± 2.082	0.311 ± 0.010
700 µg:1.5 mg	95.8 ± 1.607	32 ± 2.517	0.363 ± 0.021
1.5 mg:1 mg	103.6 ± 1.528	31.4 ± 1.026	0.39 ± 0.025
1.5 mg:2 mg	109.8 ± 1.756	30.5 ± 1.258	0.418 ± 0.010
900 µg:1 mg	91 ± 2.0	30 ± 1.528	0.69 ± 0.010
0.5 mg:0.5 mg	102 ± 2.517	34.5 ± 2.255	0.471 ± 0.017
1.3 mg:1 mg	112.6 ± 2.517	29 ± 1.528	0.891 ± 0.010

be different, fluorescence emission spectra cannot evaluate the amount of drug inside the micelles. As US exerts pressure on micelles, population distribution changes from homogeneous to heterogeneous. Interestingly, upon ultrasound exposure, the distinct fluorescence peak of Dox reappears in the photoluminescence spectra, showing the release of drug from nanomicelles and breakage of polymer drug conjugation. Photoluminescence explains the energy transfer mechanism between the hDox and PmGCA, which occurs when a photon is released upon relaxation of an electron from excitation state. In previous study, scientists have correlated the change in photoluminescence with the degree of chemical bonding of Dox to the salmon DNA molecule [37]. Huang et al. have explored the quenching mechanism involving Dox which binds with gold nanoclusters after accepting electrons from excited gold nanoclusters and quenching their fluorescence through photoluminescence [38]. Based on this, we hypothesize that our polymer encapsulates hDox and quenches fluorescence.

Stability study

Palmitoyl glycol chitosan amphiphile micelles can encapsulate 210 ± 0.05 µg which is 70% of the initial hydrophobic doxorubicin quantity. This is due to the hydrophobic pendants of palmitoyl groups, which offer excellent encapsulation to the current hydrophobic drug system. Wet stability study at 4 °C shows no significant changes in size and zeta potential up to 3 months ($p < 0.001$) (Fig. 3A). The hDox-NDS nanomicelles exhibit a small increase in average size (103 ± 1.3 nm), zeta potential (29.5 ± 1.2 mV), and PDI (0.891 ± 0.06) after being treated with serum at 37 °C for 8 h (Table 2). This slight increase in size and PDI is also observed in 99m Technetium radio-labeled palmitoyl glycol chitosan by Zia et al. (2022) [16]. In several studies [36, 39, 40], formulations including N-palmitoyl-N-monomethyl, N-N dimethyl, and N-N-N, trimethyl-6-O-glycol chitosan were found to be stable.

Hemocompatibility of hDox-NDS nanotheranostic micelles

When the concentration of nanomicelles is increased from 3, 6, 9, 12, and 18 µg, a reciprocal increase in hemolysis (%) is seen for hDox-NDS (0.5, 1.4, 3.0, 3.8, and 4.7%) and for DoxHCl (1.5, 3.1, 6, 8.3, and 12.4%) (Fig. 3B). As reported by Lu et al. doxorubicin accumulates in RBCs by increasing crystal osmotic pressure, which causes an increase in water movement inside the cells, resulting in the bursting of the cell membrane [41]. Blank PmGCA shows hemocompatible with 0.69, 1.1, 2.8, 3.5, and 3.9% hemolysis against same concentrations ($p < 0.05$). The effects of hDox-NDS are found to be non-hemolytic and very consistent with the international standard of 5% toxicity as explained by Choi et al. [42]. Cationic nanomicelle interactions with negatively charged cell membrane surfaces allow easy translocation across cell membrane and a high degree of cellular internalization. This property makes cationic nanomicelles a preferable drug carrier. Several studies have confirmed the biocompatibility of polymer [17, 43]. The possible reported mechanism is that polymer inhibits breakage and solubilization of the red blood cell membrane [17, 44]. So, hDox-NDS nanomicelles cause minimal damage to red blood cells, indicating safety for in vivo administration.

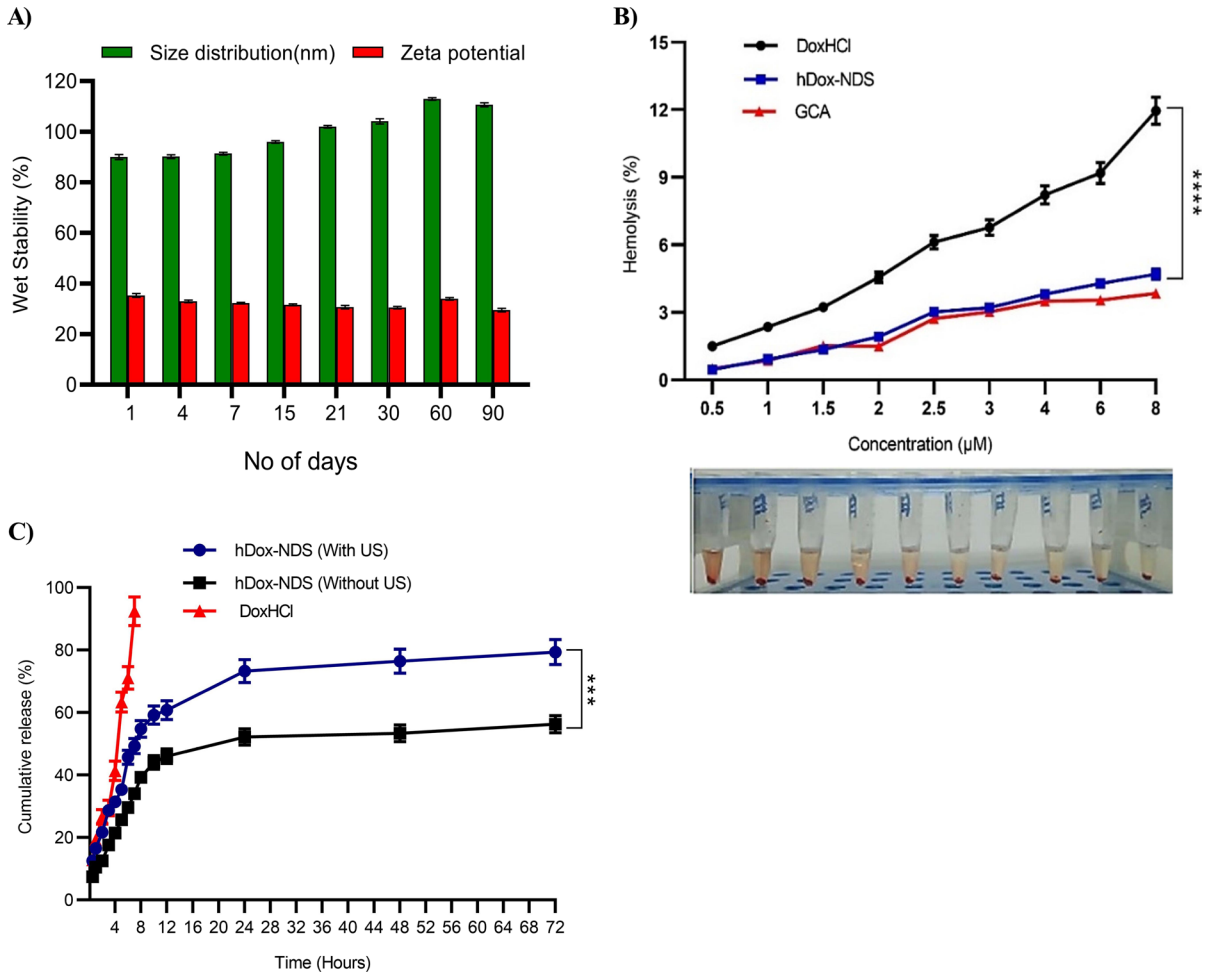

Fig. 3 Wet stability, hemolysis, and in vitro release study of hDox-NDS nanomicelles. **A** Wet stability study of Dox encapsulated PmGCA (hDox-NDS). **B** Hemolytic activity of Dox-HCl; hDox-NDS, PmGCA against human RBCs (0.5–8 μg). **C** In vitro release profile of doxorubicin hDox-NDS (with and without US; $p < 0.001$) and DoxHCl

Table 2 Particle size, zeta potential, and PDI of nanomicelles in water and FBS

Sample	Water			10% FBS		
	Size (nm)	Zeta potential (mV)	PDI	Size (nm)	Zeta potential (mV)	PDI
1	99 ± 1.2	+35.8 ± 1.03	0.224 ± 0.016	95 ± 2.0	+30.2 ± 1.2	0.246 ± 0.015
2	96 ± 4.2	+34.1 ± 2.1	0.227 ± 0.015	97 ± 3.1	+32.5 ± 1.1	0.278 ± 0.021
3	100 ± 1.5	+29.5 ± 1.2	0.235 ± 0.013	99 ± 1.3	+34.8 ± 1.02	0.28 ± 0.011
4	103 ± 1.3	+29.9 ± 1.9	0.291 ± 0.011	101 ± 4.5	+29.5 ± 2.1	0.891 ± 0.006

Ultrasound effect on release kinetics of doxorubicin

When hDox-NDS is stimulated by ultrasound, there is a noticeable increase in drug release. At stimulation points, ultrasound disrupts the nanomicelles and releases the payload. The cumulative release (%) at 0.5, 3, 6, and 24 h is 7.43, 17.62, 29.59, and 52.22% without ultrasound and 12.54,

28.73, 45.69, and 73.32% with ultrasound. The initial concentration of encapsulated nanomicelles is 210 ± 0.05 µg. The measured concentrations are 26.34, 60.35, 95.95, and 153.9 µg and 15.6, 37.01, 62.14, and 109.6 µg with and without US, respectively, at each time point. Following exposure to ultrasound, there is an increase in drug release of 51.10, 47.93, 42.77, and 33.61% after 72 h (Fig. 3C). R square values for US-mediated hDox-NDS release vs no US–mediated release in six kinetic release models applied are as follows: zero order −1.0487 vs −0.8080), Korsmeyer-Peppas (0.8826 vs 0.8464), Weibull (0.991 vs 0.997), Hixson-Crowell (0.5597 vs −0.1961), Higuchi (0.5845 vs 0.6141), and first order (0.7856 vs 0.1138) (Table S3).

The Weibull model is found to be more appropriate for US-mediated cumulative release from hDox-NDS nanomicelles, which correlates to immediate and regulated drug release [45]. The observed β value of 0.500 (US) and 0.398 (no US) show immediate release of drug. As indicated by Herdiana et al. value of $\beta > 1$ results in a sigmoidal release curve with a turning point in the initial phase, a value of $\beta < 1$ results in a sharper climb, and a value of $\beta = 1$ results in an exponential increase in the release slope [46]. Li et al. have stated that micelles of a less hydrophilic character are more sensitive to ultrasound than more hydrophilic moieties [26, 47]. PmGCA cationic charge on surface of micelles rendered by quaternary ammonium groups makes it more susceptible to ultrasound exposure. The hydrophobic core of palmitoyl pendants can cause low water activity within the core, thus offering stability to the hDox-NDS nanomicelles [48].

Higher fluorescence in RD cells corresponds to more Dox uptake after US exposure

A marked increase in fluorescence intensity in US-exposed cells corresponds to higher drug uptake as compared to non-exposed cells. A 30-s exposure of 2 MHz with MI of 1.2 significantly improves the penetration of nanotheranostic micelles in cell monolayers in hDox-NDS+US group ($p < 0.001$). Fluorescence intensity increases from 1.0×10^7 to 1.12×10^7 which corresponds to ~10% increase. This increase in fluorescence may be explained due to enhanced penetration of hDox-NDS after exposure of cells to US, as demonstrated by fluorescence microscopy. Enhanced penetration of hDOx-NDS in cells is due to the application of ultrasound which created pores in the cell membrane for maximum release of the drug at the site of action. As less fluorescence is observed in cells without US exposure (Fig. 4A, B), DoxHCl shows 8.1×10^6 vs 4.5×10^5 fluorescence intensity in the US vs without US exposed cells ($p < 0.001$). According to Xiong et al. ultrasound may widen the intercellular gaps due to the disruption of desmosomes connecting the cells, thus enhancing penetration of hDox-NDS nanomicelles [49]. This also demonstrates hDox-NDS's good dispersal stability, which helps to localized delivery. When compared to DoxHCl, which was internalized by the cells through simple diffusion, hDox-NDS shows greater penetration, which improves its cytotoxicity toward tumor cells. The exposure to the US is thought to have caused the caveolae-mediated endocytosis. It is also assumed that ultrasonic waves may increase the rate of internalization of preformed caveolae via caveolin-1 phosphorylation. It is reported that numerous US-generated mechanical stresses may combine to produce effects that induce significant changes in the membrane and molecular structures of cells, thus causing internalization of nanoparticles [48]. Besides that, a size of less than 100 nm has also demonstrated excellent endocytosis by cells, as reported by Afshari et al. [14].

Macrophage uptake of hDox-NDS nanotheranostic micelles after US exposure

In human macrophage cells, our less than 100-nm cationic hDox-NDS is poorly absorbed when exposed to US, whereas DoxHCl is readily absorbed regardless of exposure. Macrophages consider nanoparticles as foreign bodies if their particle size is greater than 200 nm. Nanomicelles with a size below 100 nanometers are less likely to enter macrophage cells (Fig. 4A). It has been documented by Champion et al. that endocytosis by macrophages is affected by the size and surface morphology of particles. hDox-NDS particle size and positive zeta potential contribute to its stability and prevent it from interacting with phagocytic system of the body. It results in less uptake by macrophage defense system, thus

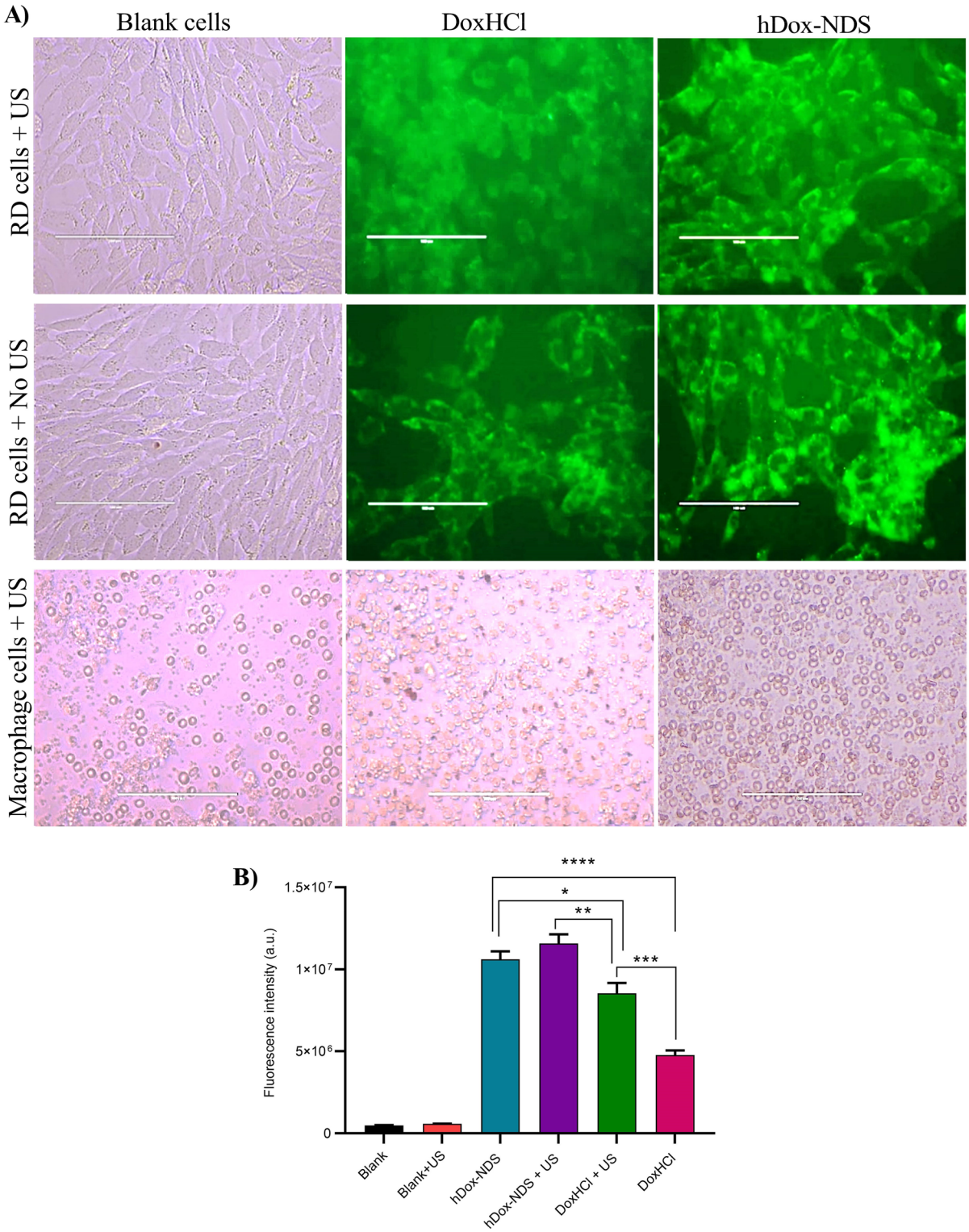

Fig. 4 Effects of ultrasound on Dox/hDox-NDS uptake in rhabdomyosarcoma cells and macrophages. **A** Enhanced uptake is observed after US exposure. Images taken at 20X transmitted/GFP filter using EVOS, FL cell imaging system. **B** Fluorescence intensity graph of cell uptake study

improving circulation and nonspecific distribution in healthy organs. Using a receptor-mediated procedure, micron-size particles are picked up by macrophages in the liver and spleen and absorbed through an actin-driven process [50]. So larger size and hydrophobicity cause increase in phagocytosis. According to Fang et al. link between cell size and phagocytosis influences cell surface interaction, causing immunological response [51]. Interestingly, Jiang et al. have reported sphere shape particles are internalized at a slower rate by macrophages as compared to rod shaped particles [50, 52]. Previous literature has shown more efficient uptake of larger particles than of small size particles of same composition and surface morphology. Gabizon et al. stated that nanoparticles of 50–200 nm are recommended for extending systemic circulation time, but nanoparticles larger than 500 nm are primarily eliminated via macrophages [6]. Due to their virtually spherical shape, hDox-NDs are therefore less likely to be swallowed by macrophages. Alqahtani et al. [53] stated larger gliadin nanoparticles of more than 406 nm ± 11 have shown higher macrophage uptake, while smaller particles of size 127 nm ± 8 show minimal uptake. As a result, the drug will be available for absorption in the circulatory system for a longer period. So, less phagocytosis by macrophages gives nanomicelles longer circulation time [51, 53, 54].

Phantom model shows extravasation after ultrasound exposure

A clear, visible extravasation is recorded when ultrasound is applied to phantom channels after hDox-NDS injection. Sonograms reveal outflow of nanomicelles and seepage of Dox after ultrasound application in the form of white streaks at a depth of 1.5 cm, while drug remains in channels when no US is applied (Fig. 5A–G). This indicates the penetration and rupture of cationic nanomicelles upon US application. Our results are consistent with those of Nittayacharn et al. (2022) that reports gold nanocones help in substantial increase in penetration of therapeutic agent in a tissue-imitating phantom at a distance of more than 2 mm during the in vitro extravasation studies. A similar outcome is anticipated in vivo. Possibly, ultrasound generates sound waves that can induce cavitation, which helps in the release of drugs from polymer at the site of action [55].

Ultrasound exposure lowers IC_{50} value of hDox-NDS nanotheranostic micelles

The findings support a dose-dependent response of cells to hDox-NDS in reducing cancer cell proliferation. hDox-NDS exhibits 91.9–62.76% viability, whereas DoxHCl shows 98–59% viability against 0.5, 1, 1.5, 2, 2.5, 3, 3.5, 4, 4.5, 4.9, and 5 µM concentration. Cell micrographs show fewer live cells in hDox-NDS group, as compared to more live cells at the same DoxHCl. When compared to DoxHCl, hDox-NDS is more toxic to cancer cells. hDox-NDS has an IC_{50} of 2.62 ± 1.2 µM without US, whereas DoxHCl has an IC_{50} of 3.9 ± 1.2 µM. Statistically significant decrease in IC_{50} values of hDox-NDS vs DoxHCl is observed after ultrasound exposure, i.e., 1.7 ± 0.05 µM vs 3.85 ± 0.3 µM ($p < 0.001$), against RD cells (Fig. 6A, B). Fant C et al. also found lower cell viability in groups exposed to US. It is hypothesized that once internalized, nanomicelles will break down due to US exposure and release their payload, increasing cytotoxicity [56].

Less cell survival is observed after US exposure

hDox-NDS + US treated group has less cell survival (17%) than no US-treated group (27.5%) at 2 MHz (1.2 MI) for 30 s. DoxHCl + US shows 44% vs 66.3% cell survival in no US group. Under the aforementioned conditions, 97% of cells in control group survive after US exposure (Fig. 6C). Based on these results, we assume that the use of US is safe for use in cells. FDA has also established a threshold limit of less than 1.9 MI for use in animal models [31]. The hDox-NDS + US group exhibits a considerable drop in cell count. Laing et al. reported a decrease in cell survival after 20 s 1-MHz US exposure. They have also stated the reciprocal effects of intensity and exposure time of US on cell survival [57]. Jawaid et al. have reported that the US enhances the killing effects of platinum nanoparticles at 1 MHz for 2 min of exposure upon internalization in the cell. So, it can be speculated that US helps in drug penetration, resulting in drug efficacy [34].

In vivo biodistribution of hDox-NDS nanotheranostic micelles

The biodistribution pattern of hDox-NDS group in terms of fluorescence measurements without US is less compared to ultrasound exposure. The fluorescence

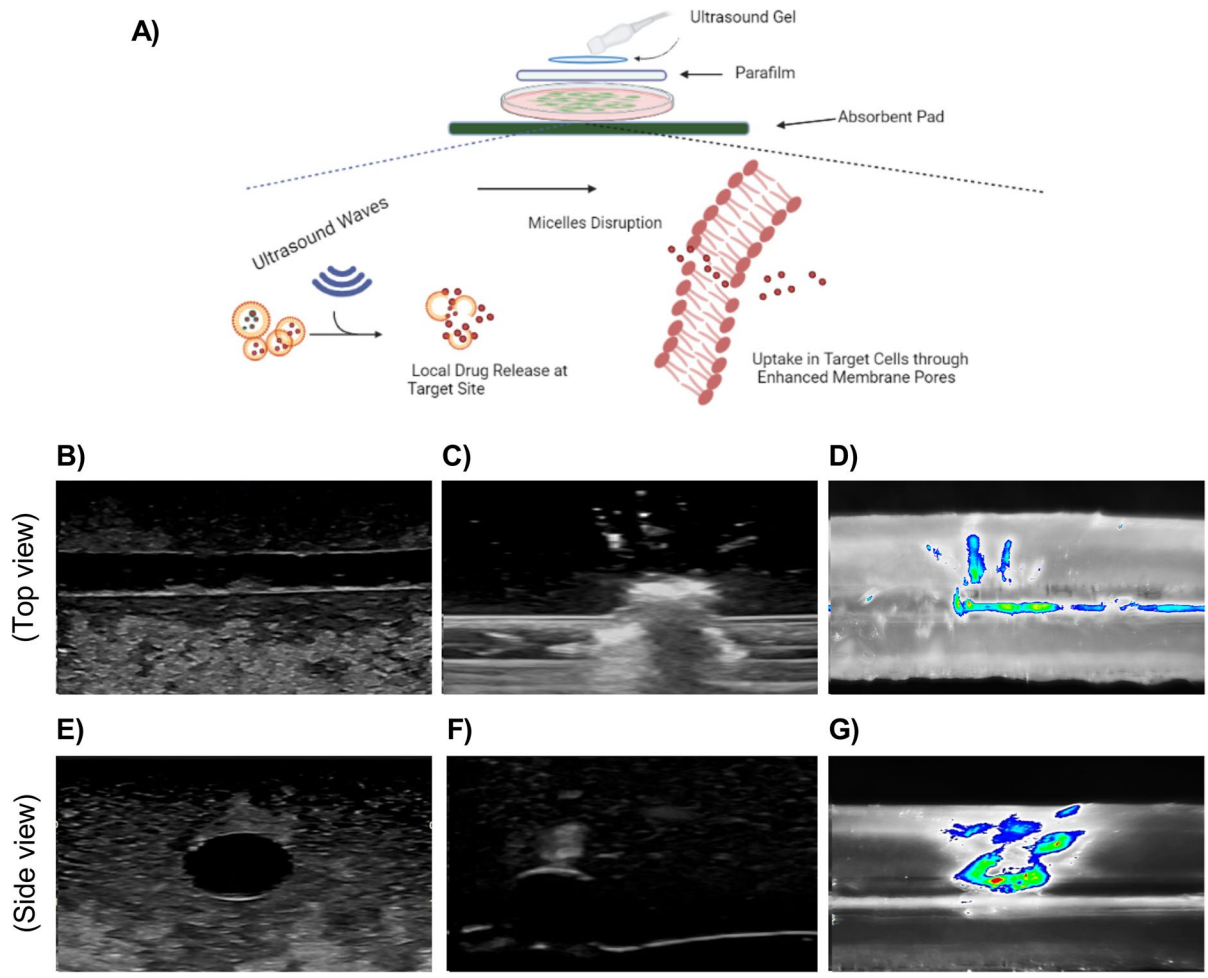

Fig. 5 Ultrasound-mediated enhanced penetration of hDox-NDS in a gel phantom model. **A** Graphical presentation of cell uptake with ultrasound. **B–D** B-mode images of hDox-NDS injected gel phantom before 30 s of ultrasound exposure (top view). **E–F** B-mode images of hDox-NDS injected gel phantom after 30 s of US exposure showing drug penetration (side view)

intensity values of hDox-NDS with and without ultrasound are mentioned in Table S4 and Fig. 7. Overall, this difference is statistically significant with $p < 0.001$ in the US-exposed hDox-NDS group. Major issues of cardiotoxicity related to commercially available doxorubicin may be overcome by encapsulation in hDox-NDS which shows 84% less drug uptake in the heart (Fig. 8). Due to the presence of hydrophobic and hydrophilic group and ease of alteration in biodistribution due to the availability of functional groups, PmGCA is one of the best nanocarriers [16, 39]. The change in the route of biodistribution of Dox is mostly due to a decrease in PmGCA polymer uptake in the liver. Ultimately, this reduced liver uptake and escape from enzymatic degradation will favor Dox distribution to the brain and later the kidney for clearance, because less than 100-nm particles are thought to be cleared through renal routes. In addition, when combined with US hDox-NDS, nanomicelles (< 100 nm) become more penetrable to the target tissue. Foroozandeh and Aziz (2018) discovered that smaller molecules (< 200 nm) accumulate faster in the tumor cells [47]. According to Liu et al. 60% of 100–200-nm particles are found in circulation, compared to only 20% of < 50-nm and > 250-nm particles. In line with the expected route of excretion for hydrophilic polymeric compounds, renal routes represent a primary route of excretion. One of our recently published studies found

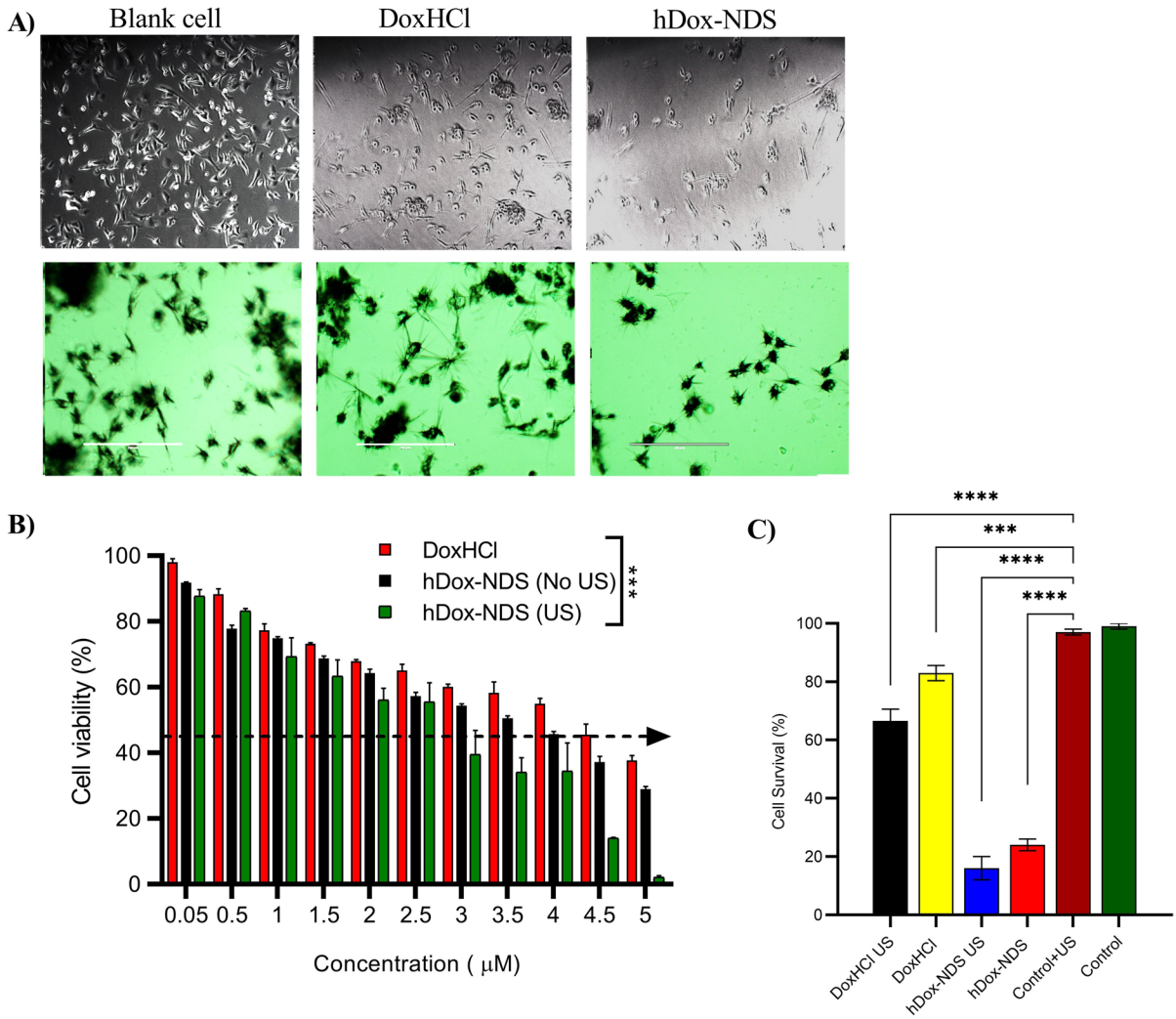

Fig. 6 Effect of ultrasound on viability of rhabdomyosarcoma cells treated with DoxHCl/hDox-NDS. **A** RD cells images with inverted microscope after incubation with hDox-NDS/DoxHCl. **B** Percent cell viability after 48 h of incubation. **C** Cell survival (%) through trypan blue assay of DoxHCl/hDox-NDS-treated rhabdomyosarcoma cells

a substantial amount of radioactivity-labeled polymer PmGCA in the bladder, which indicates that major excretion route is renal [16]. Our findings are supported by multiple studies with PmGCA where intravenous distribution kinetics prevented the uptake by the liver and spleen [18, 58, 59]. Interestingly, hDox-NDS crosses blood-brain barrier, which otherwise remains impermeable to DoxHCl. This can be correlated to polymer's ability to cross the blood-brain barrier, thus making it a good tool for carrying the drug to the gliomas. One of the previous studies has reported the presence of delta opioid receptors throughout the central nervous system, due to which PmGCA is internalized by brain cells. We therefore have adequate evidence to claim that intravenously administered nanoparticles coated with PmGCA will likewise be able to bind to delta opioid receptors [18].

In vivo histopathological examination

In all groups, no hemorrhage or other acute tissue damage is noticed in hematoxylin-eosin–stained specimens. There is no parenchymal distortion, fibrosis, or vascular anomaly in the hDox-NDS

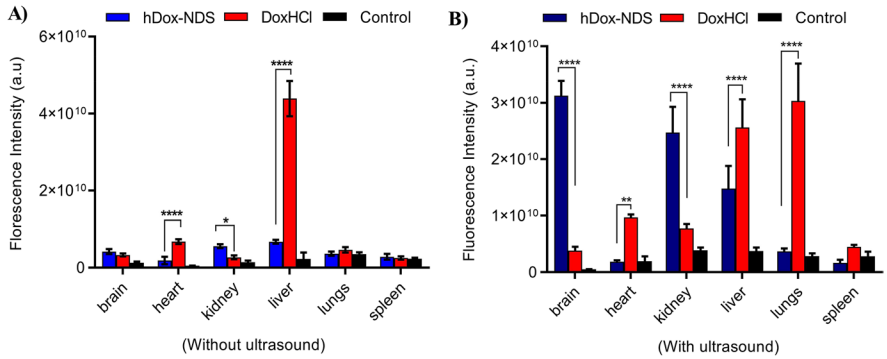

Fig. 7 Fluorescence intensities (FI) of mice organs after ultrasound exposure post DoxHCl/hDox-NDS injection. **A** Fluorescence intensity without ultrasound. **B** Fluorescence intensity with ultrasound. Images were taken at 535/45 excitation and 605/50 emission filter with imaging system UVP iBOX® Explorer2™ Imaging Microscope Analytik Jena, CA (USA). $****p < 0.0001$, $***p < 0.001$, $**p < 0.01$,$*p < 0.05$

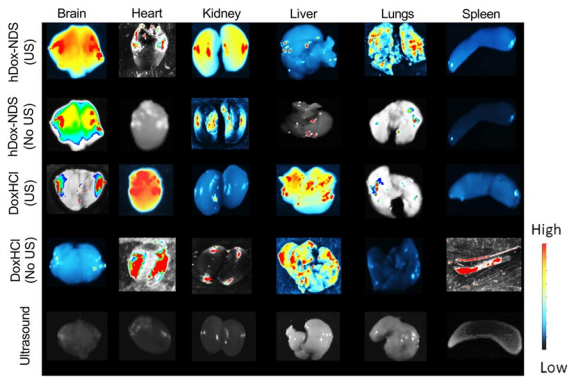

Fig. 8 Biodistribution of intravenously injected DoxHCl/hDox-NDS, with/without ultrasound exposure through an optical imaging system in mice organs (injected dose 0.05/g). Fluorescence intensity of organs taken after intraperitoneal drug injection, without ultrasound stimulation (fluorescence intensity range highest to lowest is 65535-0). Images were taken at 535/45 excitation and 605/50 emission filter with Bioautomatic MultiSpectral Light Source using in vivo small animal imaging system UVP iBox® Explorer2™ Imaging Microscope Analytik Jena, CA (USA). FI is a corrected value by taking background noise into consideration

group. No hepatic cell abnormality is being recorded in the liver with or without ultrasound exposure in hDox-NDS. Besides that, no heart damage or acute cardiotoxicity is observed in the ultrasound exposed hDox-NDS nanomicelle group. However, slight heart congestion is visible in the DoxHCl-exposed group compared to the hDox-NDS group as well as from fluorescence imaging through the whole body imaging system. This is most likely due to a change in drug behavior caused by the nanomicellar carrier as well as an ultrasound trigger, which alters the route of drug distribution, as demonstrated by a biodistribution study. After treating mouse organs with hDox-NDS nanomicelles, no obvious tissue abnormalities or lesions are observed, demonstrating their low biotoxicity. Overall, no tissue damage is observed in any organ in the hDox-NDS group as seen in the photomicrograph (Fig. 9). The negligible toxicity values show that PmGCA nanoparticles are not recognized as foreign via the mammalian immune system [17]. Our results are in close agreement with that of Uchegbu et al., which also stated the biocompatible nature of palmitoyl glycol chitosan [36]. Furthermore, Lalatsa et al. reported that this polymer has negligible toxicity toward healthy tissues [44].

Conclusion

In conclusion, we have developed a US-responsive nanomicelle drug delivery system (hDox-NDS) for highly effective chemotherapy. The PmGCA in the polymeric micelle structure can protect the adsorption of Dox in the blood circulation, retaining a firm nanostructure for better tumor targeting and minimizing the harmful effects of Dox. Moreover, drug-loaded micelles can attain enhanced accumulation at the tumor site due to EPR effect. Following US application, the micelles at the target site underwent a responsive structural change,

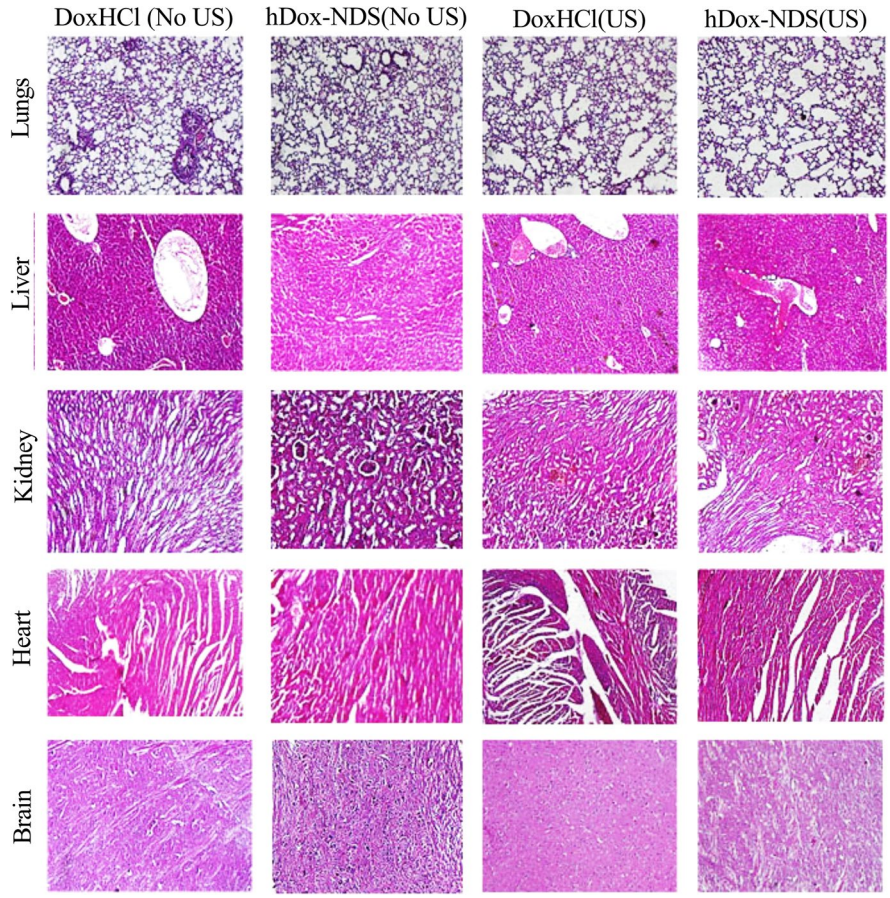

Fig. 9 Histopathology of DoxHCl, hDox-NDS (0.05 µg/g) with/without ultrasound exposure in BALB/c mice organs. H&E staining of paraffin section to observe biodistribution of drug (DoxHCl/ hDox-NDS)

peeling the PmGCA and promptly releasing the medication, facilitating doxorubicin easier uptake by the target cells, and enhancing chemotherapeutic efficiency. The study's findings showed that hDox-NDS has a stronger anticancer effect and sensitive US response characteristics, as well enhanced cellular absorption and favorable biosafety. The coherent design of US-responsive nanoparticles represents a promising model for very effective in vivo targeted distribution of anticancer agents and potentially provides a complementary choice for better chemotherapy efficacy.

Acknowledgements Chemicals and equipment used in the research work are supported through the PAK-NORWAY Institutional Cooperation Program, PK3004, COMSTECH-TWAS (12-198 RG/PHA/AS_C-UNESCO FR: 3240270874), and Pakistan Science Foundation (PSF/Res/C-NILOP/Med (330). The authors are grateful to the Pakistan Institute of Applied Sciences (PIEAS) and the National Institute of Health (NIH) for technical support.

Compliance with ethical standards

Conflict of interest The authors declare no competing interests.

References

1. Ladju RB, Ulhaq ZS, Soraya GV (2022) Nanotheranostics: a powerful next-generation solution to tackle hepatocellular carcinoma. World J Gastroenterol 28:176
2. Afadzi M, Myhre OF, Yemane PT et al (2020) Effect of acoustic radiation force on the distribution of nanoparticles in solid tumors. IEEE Trans Ultrason Ferroelectr Freq Control 68:432–445
3. Kim D, Lee JH, Moon H et al (2021) Development and evaluation of an ultrasound-triggered microbubble combined transarterial chemoembolization (TACE) formulation on rabbit VX2 liver cancer model. Theranostics 11:79
4. Young RC, Ozols RF, Myers CE (1981) The anthracycline antineoplastic drugs. N Engl J Med 305:139–153
5. Melim C, Magalhães M, Santos AC et al (2022) Nanoparticles as phytochemical carriers for cancer treatment: news of the last decade. Expert Opin Drug Deliv 19:179–197

6. Gabizon A, Shmeeda H, Barenholz Y (2003) Pharmacokinetics of pegylated liposomal doxorubicin. Clin Pharmacokinet 42:419–436
7. Hekmatirad S, Moloudizargari M, Moghadamnia AA et al (2021) Inhibition of exosome release sensitizes U937 cells to PEGylated liposomal doxorubicin. Front Immunol 12:2008
8. Hilger RA, Richly H, Grubert M et al (2005) Pharmacokinetics (PK) of a liposomal encapsulated fraction containing doxorubicin and of doxorubicin released from the liposomal capsule after intravenous infusion of Caelyx/Doxil. Int J Clin Pharmacol Ther 43:588–589
9. Liu L, Kshirsagar PG, Gautam SK et al (2022) Nanocarriers for pancreatic cancer imaging, treatments, and immunotherapies. Theranostics 12:1030
10. Entzian K, Aigner A (2021) Drug delivery by ultrasound-responsive nanocarriers for cancer treatment. Pharmaceutics 13:1135
11. Mohan P, Rapoport N (2010) Doxorubicin as a molecular nanotheranostic agent: effect of doxorubicin encapsulation in micelles or nanoemulsions on the ultrasound-mediated intracellular delivery and nuclear trafficking. Mol Pharm 7:1959–1973
12. Mi P (2020) Stimuli-responsive nanocarriers for drug delivery, tumor imaging, therapy and theranostics. Theranostics 10:4557
13. Behera SK, Mohanty ME, Mohapatra M (2021) A fluorescence study of the interaction of anticancer drug molecule doxorubicin hydrochloride in pluronic P123 and F127 micelles. J Fluoresc 31:17–27
14. Afshari AR, Sanati M, Mollazadeh H et al (2022) Nanoparticle-based drug delivery systems in cancer: a focus on inflammatory pathways. Semin Cancer Biol. https://doi.org/10.1016/j.semcancer.2022.01.008
15. Xia H, Yang D, He W et al (2021) Ultrasound-mediated microbubbles cavitation enhanced chemotherapy of advanced prostate cancer by increasing the permeability of blood-prostate barrier. Transl Oncol 14:101177
16. Zia N, Iqbal Z, Raza A et al (2022) Glycol-chitosan-based Technetium-99m-loaded multifunctional nanomicelles: synthesis, evaluation, and in vivo biodistribution. Nanomaterials 12:2198. https://doi.org/10.3390/nano12132198
17. Uchegbu IF, Sadiq L, Arastoo M et al (2001) Quaternary ammonium palmitoyl glycol chitosan—a new polysoap for drug delivery. Int J Pharm 224:185–199
18. Lalatsa A, Schätzlein AG, Garrett NL et al (2015) Chitosan amphiphile coating of peptide nanofibres reduces liver uptake and delivers the peptide to the brain on intravenous administration. J Controlled Release 197:87–96. https://doi.org/10.1016/j.jconrel.2014.10.028
19. Min HS, You DG, Son S et al (2015) Echogenic glycol chitosan nanoparticles for ultrasound-triggered cancer Theranostics. Theranostics 5:1402–1418. https://doi.org/10.7150/thno.13099
20. Zhou X, Guo L, Shi D et al (2019) Biocompatible chitosan nanobubbles for ultrasound-mediated targeted delivery of doxorubicin. Nanoscale Res Lett 14:24. https://doi.org/10.1186/s11671-019-2853-x
21. Meng D, Guo L, Shi D et al (2019) Charge-conversion and ultrasound-responsive O-carboxymethyl chitosan nanodroplets for controlled drug delivery. Nanomed 14:2549–2565
22. Kanwal U, Bukhari NI, Rana NF et al (2019) Doxorubicin-loaded quaternary ammonium palmitoyl glycol chitosan polymeric nanoformulation: uptake by cells and organs. Int J Nanomedicine 14:1–15
23. Wei T, Chen C, Liu J et al (2015) Anticancer drug nanomicelles formed by self-assembling amphiphilic dendrimer to combat cancer drug resistance. Proc Natl Acad Sci 112:2978–2983
24. Khan MA, Ansari MM, Arif ST et al (2021) Eplerenone nanocrystals engineered by controlled crystallization for enhanced oral bioavailability. Drug Deliv 28:2510–2524
25. Ovais M, Nadhman A, Khalil AT et al (2017) Biosynthesized colloidal silver and gold nanoparticles as emerging leishmanicidal agents: an insight. Nanomed 12:2807–2819
26. Li K, Li P, Jia Z et al (2018) Enhanced fluorescent intensity of magnetic-fluorescent bifunctional PLGA microspheres based on Janus electrospraying for bioapplication. Sci Rep 8:1–11
27. Rehman M, Raza A, Khan JA, Zia MA (2021) Laser responsive cisplatin-gold nano-assembly synergizes the effect of cisplatin with compliance. J Pharm Sci 110:1749–1760
28. Mannaris C, Teo BM, Seth A et al (2018) Gas-stabilizing gold nanocones for acoustically mediated drug delivery. Adv Healthc Mater 7:1800184
29. Sarwar U, Naeem M, Nurjis F, et al (2022) Ultrasound-mediated in vivo biodistribution of coumarin-labeled sorafenib-loaded liposome-based nanotheranostic system. Nanomed 17:1909–1927
30. Salgarella AR, Zahoranová A, Šrámková P et al (2018) Investigation of drug release modulation from poly (2-oxazoline) micelles through ultrasound. Sci Rep 8:1–13
31. Nelson TR, Fowlkes JB, Abramowicz JS, Church CC (2009) Ultrasound biosafety considerations for the practicing sonographer and sonologist. J Ultrasound Med 28:139–150. https://doi.org/10.7863/jum.2009.28.2.139
32. Schneider CA, Rasband WS, Eliceiri KW (2012) NIH Image to ImageJ: 25 years of image analysis. Nat Methods 9:671–675
33. Lefort CT, Kim M (2010) Human T lymphocyte isolation, culture and analysis of migration in vitro. JoVE J Vis Exp e2017
34. Jawaid P, Rehman MU, Hassan MA et al (2016) Effect of platinum nanoparticles on cell death induced by ultrasound in human lymphoma U937 cells. Ultrason Sonochem 31:206–215. https://doi.org/10.1016/j.ultsonch.2015.12.013
35. Esmaeilzadeh-Gharedaghi E, Faramarzi MA, Amini MA et al (2012) Effects of processing parameters on particle size of ultrasound prepared chitosan nanoparticles: an artificial neural networks study. Pharm Dev Technol 17:638–647
36. Uchegbu IF, Breznikar J, Zaffalon A et al (2021) Polymeric micelles for the enhanced deposition of hydrophobic drugs into ocular tissues, without plasma exposure. Pharmaceutics 13:744
37. Gnapareddy B, Reddy Dugasani S, Ha T et al (2015) Chemical and physical characteristics of doxorubicin hydrochloride drug-doped salmon DNA thin films. Sci Rep 5:1–9
38. Huang K-Y, He H-X, He S-B et al (2019) Gold nanocluster-based fluorescence turn-off probe for sensing of doxorubicin by photoinduced electron transfer. Sens Actuators B Chem 296:126656

39. Chooi KW, Carlos MIS, Soundararajan R et al (2014) Physical characterisation and long-term stability studies on quaternary ammonium palmitoyl glycol chitosan (GCPQ)—a new drug delivery polymer. J Pharm Sci 103:2296–2306
40. Lu Y, Zhang E, Yang J, Cao Z (2018) Strategies to improve micelle stability for drug delivery. Nano Res 11:4985–4998. https://doi.org/10.1007/s12274-018-2152-3
41. Lu D, Wen X, Liang J et al (2009) A pH-sensitive nano drug delivery system derived from pullulan/doxorubicin conjugate. J Biomed Mater Res B Appl Biomater 89B:177–183. https://doi.org/10.1002/jbm.b.31203
42. Choi J-S, Park J-W, Seu Y-B, Doh K-O (2021) Enhanced efficacy of folate-incorporated cholesteryl doxorubicin liposome in folate receptor abundant cancer cell. J Drug Deliv Sci Technol 62:102385
43. Wu P, Jia Y, Qu F et al (2017) Ultrasound-responsive polymeric micelles for sonoporation-assisted site-specific therapeutic action. ACS Appl Mater Interfaces 9:25706–25716
44. Lalatsa A, Schatzlein AG, Uchegbu IF (2014) Strategies to deliver peptide drugs to the brain. Mol Pharm 11:1081–1093
45. Izci M, Maksoudian C, Manshian BB, Soenen SJ (2021) The use of alternative strategies for enhanced nanoparticle delivery to solid tumors. Chem Rev 121:1746–1803
46. Herdiana Y, Wathoni N, Shamsuddin S, Muchtaridi M (2022) Drug release study of the chitosan-based nanoparticles. Heliyon 8:e08674. https://doi.org/10.1016/j.heliyon.2021.e08674
47. Foroozandeh P, Aziz AA (2018) Insight into cellular uptake and intracellular trafficking of nanoparticles. Nanoscale Res Lett 13:1–12
48. Snipstad S, Berg S, Mørch Ý et al (2017) Ultrasound improves the delivery and therapeutic effect of nanoparticle-stabilized microbubbles in breast cancer xenografts. Ultrasound Med Biol 43:2651–2669
49. Xiong R, Xu RX, Huang C et al (2021) Stimuli-responsive nanobubbles for biomedical applications. Chem Soc Rev 50:5746–5776
50. Champion JA, Walker A, Mitragotri S (2008) Role of particle size in phagocytosis of polymeric microspheres. Pharm Res 25:1815–1821
51. Fang C, Kievit FM, Cho Y-C et al (2012) Effect of cationic side-chains on intracellular delivery and cytotoxicity of pH sensitive polymer–doxorubicin nanocarriers. Nanoscale 4:7012–7020
52. Jiang LQ, Wang TY, Webster TJ et al (2017) Intracellular disposition of chitosan nanoparticles in macrophages: intracellular uptake, exocytosis, and intercellular transport. Int J Nanomedicine 12:6383
53. Alqahtani MS, Syed R, Alshehri M (2020) Size-dependent phagocytic uptake and immunogenicity of gliadin nanoparticles. Polymers 12:2576
54. Vonarbourg A, Passirani C, Saulnier P, Benoit J-P (2006) Parameters influencing the stealthiness of colloidal drug delivery systems. Biomaterials 27:4356–4373
55. Nittayacharn P, Yuan H-X, Hernandez C et al (2019) Enhancing tumor drug distribution with ultrasound-triggered nanobubbles. J Pharm Sci 108:3091–3098
56. Fant C, Lafond M, Rogez B et al (2019) In vitro potentiation of doxorubicin by unseeded controlled non-inertial ultrasound cavitation. Sci Rep 9:15581. https://doi.org/10.1038/s41598-019-51785-7
57. Liang H-D, Lu QL, Xue S-A et al (2004) Optimisation of ultrasound-mediated gene transfer (sonoporation) in skeletal muscle cells. Ultrasound Med Biol 30:1523–1529. https://doi.org/10.1016/j.ultrasmedbio.2004.08.021
58. Zhang Z, Wang Y, Ma Q et al (2021) Biomimetic carrier-free nanoparticle delivers digoxin and doxorubicin to exhibit synergetic antitumor activity in vitro and in vivo. Chem Eng J 406:126801
59. Liu D, Mori A, Huang L (1992) Role of liposome size and RES blockade in controlling biodistribution and tumor uptake of GM1-containing liposomes. Biochim Biophys Acta BBA - Biomembr 1104:95–101. https://doi.org/10.1016/0005-2736(92)90136-A